Optics Letters

Strong exciton–plasmon coupling in dye-doped film on a planar hyperbolic metamaterial

E. K. Tanyi,[1,5] N. Hong,[2] T. Sawyer,[3] J. D. B. Van Schenck,[4] G. Giesbers,[4] O. Ostroverkhova,[4] and L.-J. Cheng[1,6]

[1]School of Electrical Engineering and Computer Science, Oregon State University, Corvallis, Oregon 97331, USA
[2]J. A. Woollam, Lincoln, Nebraska 68508, USA
[3]Electron Microscope Facility, Linus Pauling Science Center, Oregon State University, Corvallis, Oregon 97331, USA
[4]Department of Physics, Oregon State University, Corvallis, Oregon 97331, USA
[5]e-mail: tanyie@oregonstate.edu
[6]e-mail: chengli@oregonstate.edu

Received 20 July 2020; revised 30 September 2020; accepted 22 October 2020; posted 22 October 2020 (Doc. ID 402210); published 14 December 2020

We experimentally demonstrate the direct strong coupling between the $S_0 \rightarrow S_1$ absorption transition of rhodamine 6G (R6G) dye molecules and the surface plasmon polaritons of a hyperbolic metamaterial (HMM) substrate. The surface plasmon mode was excited by a guided mode of the R6G-doped polymer thin film on the HMM. The coupling strengths of the interactions between the surface plasmon and two molecular exciton modes are greater than the average linewidths of the individual modes indicating a strong coupling regime. This is the first, to the best of our knowledge, experimental demonstration of the direct strong coupling between the resonance mode supported by the HMM and the dye molecules on the HMM surface, not embedded in the HMM structure. The study may provide the foundation for the development of novel planar photonic or electronic devices.

https://doi.org/10.1364/OL.402210

Hyperbolic metamaterials (HMMs) are metal–dielectric composite materials engineered to exhibit hyperbolic dispersion [1–4], which implies that their effective dielectric permittivity tensors have diagonal components with different signs. HMMs possess the ability to enhance the spontaneous emission rates of emitters in the vicinity of or embedded in the metamaterials due to the increased optical density of states [1–4]. The interaction is considered a weak coupling phenomenon with no changes to the energy levels of the systems involved. On the other hand, the strong coupling regime provides the unique ability to modify the energy levels of the emitters and, hence, their absorption and emission spectra [5–7]. Recent theoretical predictions suggest the possibility of achieving the strong coupling regime even with HMMs [8–11]. Achieving strong coupling in the hyperbolic regime implies that the originally coinciding states, contributed by the surface plasmon mode on the HMM and the exciton mode from dye molecules, split into two separate polaritonic states. The unique properties resulting from the light–matter interactions may offer new possibilities for practical applications in electronic devices [12] and control of chemical reactions [13]. Although a planar metal thin film or nanopatterned metal structure can also provide surface plasmon resonances to support the strong coupling interaction, HMM has the advantage of permitting controllable optical properties by adjusting the metal filling ratio to manage the resonance mode required for efficient strong coupling, making it versatile to create devices with new functionalities. Experimental evidence of strong coupling involving HMMs has been demonstrated to assist their coupling with emitters by using nanopatterned HMMs [14] or by embedding an active layer in HMMs [8–10]. In this Letter, we demonstrate for the first time, to the best of our knowledge, the direct coupling between a dye-doped polymer and a planar multilayer HMM without the use of nanopatterns or embedding of the dye molecules within the HMM structure [14].

The device structure employed in this study was a multilayer HMM coated with an rhodamine 6G (R6G)-doped poly (methyl methacrylate) (PMMA) thin film [Fig. 1(a)]. The HMM layer comprised five alternating layers of 10.5 nm thick silver (Ag) and 17.7 nm thick indium tin oxide (ITO), corresponding to a metal fill fraction of 0.372, deposited on a 0.9 mm glass substrate using RF sputtering. The polymer cladding on the HMM was a 170 nm thick PMMA doped with 306 mg/ml R6G dye molecules, i.e., 3.79×10^{20} cm^{-3} in the solid PMMA. Figure 1(b) shows a cross-sectional scanning electron microscopic (SEM) image of the resulting device. The complex refractive indices of the as-deposited Ag and ITO, extracted from the ellipsometric parameters, are plotted in Fig. S1 in Supplement 1 against the data obtained by Palik [15], showing a good agreement in the general trend.

The multilayer HMM exhibits an effective anisotropic dielectric permittivity tensor $\bar{\bar{\epsilon}} = \mathrm{diag}(\epsilon_\parallel, \epsilon_\parallel, \epsilon_\perp)$, where the subscripts $\parallel$ and $\perp$ denote the components parallel and perpendicular to the multilayers (x-y plane), as depicted in Fig. 1(a). The effective permittivity components are related to the permittivity function ϵ_{Ag} (ϵ_{ITO}) and the thickness d_{Ag} (d_{ITO}) of Ag (ITO). They are given by $\epsilon_\parallel = \rho\epsilon_{\mathrm{Ag}} + (1-\rho)\epsilon_{\mathrm{ITO}}$

and $\epsilon_\perp = (\rho/\epsilon_{Ag} + (1-\rho)/\epsilon_{ITO})^{-1}$ with the fill fraction of Ag being $\rho = d_{Ag}/(d_{Ag} + d_{ITO})$. The calculated effective permittivity functions plotted in Fig. S2(a) in Supplement 1 suggest that the multilayered Ag–ITO structure with $\rho = 0.372$ in this study exhibits a hyperbolic dispersion with $\mathrm{Re}[\epsilon_\parallel] > 0$ and $\mathrm{Re}[\epsilon_\perp] < 0$ until the wavelength falls below 450 nm, at which point the epsilon-near-zero ($\epsilon_\parallel = 0$) (ENZ) occurs. The imaginary part of the permittivity functions [see Fig. S2(a) in Supplement 1] in both directions, i.e., $\mathrm{Im}[\epsilon_\parallel]$ and $\mathrm{Im}[\epsilon_\perp]$, is considerably low in the hyperbolic region, which is further confirmed by the low transmittance [Fig. S3(a)] and high reflectance [Fig. S3(b)] of the bare HMM substrate above 500 nm. The low optical absorption of the HMM substrate enables the strong interaction of the absorption bands contributed by the highly concentrated R6G dye molecules at 500 nm and 534 nm in the HMM regime.

The measured HMM transmission spectrum agrees with the theoretical prediction by the transfer matrix method (TMM), which treats the HMM as its original multilayer structure, not effective medium theory [Fig. S3(a) in Supplement 1]. The HMM reveals dielectric property at shorter wavelengths and turns metallic in the z direction after 500 nm, evidenced by the decreased transmission and increased reflectance. The PMMA cladding on the HMM in this study (Fig. 1) serves as not only a host medium for R6G dye molecules but also a slab waveguide that supports guided modes. The surface plasmon polariton (SPP) on the HMM surface can be excited by the guided mode to result in a surface plasmon resonance in a narrow wavelength range, determined by the thickness of the polymer cladding [16]. Also, without a prism or grating coupler, the guided mode can be excited from the air/PMMA interface under a sufficiently large incident angle. The Xenon light source for the ellipsometric measurements has much less power than laser. Thus, the SPP is unlikely to be excited by the scattered incident light from the unintentional scatterers in the doped PMMA layer. The thickness of the PMMA cladding was chosen to produce the SPP at the wavelength between the two exciton modes provided by R6G. The theoretical reflectance spectrum obtained by the TMM confirms that a 170 nm thick undoped PMMA on the HMM creates a resonance around 512 nm at angles of incidence larger than 75° [see Fig. S4(a) in Supplement 1]. The resonance becomes stronger and narrower as the incident angle approaches 90°, where the SPP is efficiently excited through the guided mode. This resonance lies between the two absorption peaks of the highly concentrated R6G-doped PMMA (PMMA:R6G) coated on glass [Fig. S4(b) in Supplement 1].

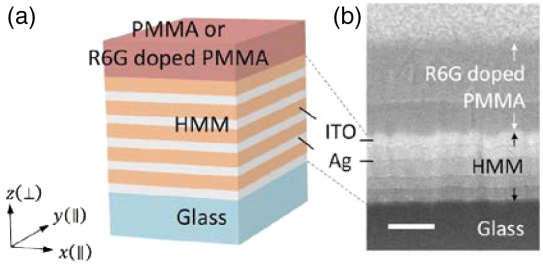

Fig. 1. (a) Schematics and (b) cross-sectional SEM image of a representative multilayer HMM coated with an R6G-doped PMMA. The HMM comprises five alternating layers of 10.5 nm Ag and 17.7 nm ITO. The scale bar in the SEM image indicates 100 nm.

For the experimental study of strong coupling, we coated a 170 nm thick R6G-doped PMMA (PMMA:R6G) layer on the HMM substrate (25 mm by 25 mm). The polymer mixture preparation and spin coating process are based on Ref. [17] and detailed in Supplement 1. Spectroscopic studies were performed using an ellipsometer to obtain the experimental reflectance spectra excited from the air/PMMA:R6G interface at various angles, ranging from 30° to 85°. The 2 mm incident beam width and the 2 mm-sized iris in front of the detector minimize the distortions arisen at large incidence angles, allowing the collection of only specular reflectance.

The exciton modes of the R6G dyes are strictly linked to the complex dielectric permittivity of the PMMA:R6G matrix $\epsilon_{ex} = \epsilon'_{ex} + i\epsilon''_{ex}$ defined by the Lorentz and Clausius–Mossotti models. With the angular frequency ω close to the absorption resonance, the real and imaginary parts of the complex dielectric permittivity can be modeled by [18]

$$\epsilon'_{ex}(\omega) = \epsilon_b + A\left(\frac{\epsilon_b + 2}{3}\right)^2 \sum_j f_j \frac{\frac{\bar{\omega}_j - \omega}{2\bar{\omega}_j}}{(\bar{\omega}_j - \omega)^2 + \left(\frac{\gamma_j}{2}\right)^2}, \quad (1)$$

$$\epsilon''_{ex}(\omega) = A\left(\frac{\epsilon_b + 2}{3}\right)^2 \sum_j f_j \frac{\frac{\gamma_j}{4\bar{\omega}_j}}{(\bar{\omega}_j - \omega)^2 + \left(\frac{\gamma_j}{2}\right)^2}, \quad (2)$$

where the subscript $j = 1, 2$ stands for exciton 1 or 2, $A = \mathrm{Ne}^2/(\mathrm{V}m\epsilon_0)$, $\bar{\omega}_j = [\omega_{0,j}^2 - A/3]^{1/2}$, $\omega_{0,j}$ is the resonance frequency of the exciton transition, γ_j is the damping frequency of the transition, and f_j is the oscillator strength of the transition. N/V is the number of R6G dye molecules per unit volume in solid-state, e and m are the charge and the mass of an electron, respectively, ϵ_0 is the vacuum permittivity, and ϵ_b is the dielectric permittivity of PMMA. The fitting parameters are summarized in Supplement 1.

Figure 2 shows the theoretical and experimental angle-dependent reflectance spectra of the PMMA:R6G coated HMM sample for p-polarized light. Both plots display two main angle-independent dips at about 500 nm and 534 nm, indicated by the green squares and blue triangles for angles less than 75°. The two dips are associated with the original two molecular exciton modes of R6G at 504 nm and 550 nm measured through a normal transmission on glass [Fig. S4(b) in Supplement 1]. The slight difference between the exciton levels measured on glass (at 504 nm and at 550 nm) and those on the HMM (at 500 nm and at 534 nm) may be due to the effect of the substrate materials on the orientation of the dipole moments of each exciton transition [19,20]. It could also result from the different characterization conditions—the exciton levels of the R6G on glass were obtained from the normal transmission spectrum at 0°, whereas the results on HMM were acquired using angle-dependent reflectance spectra with incident angles greater than 30°. The two R6G exciton modes remain unchanged at small incident angles where no SPP is available for strong coupling (Fig. 2). As the incident angle increases beyond 75°, the two reflectance dips move further apart and become more pronounced; meanwhile, a third minor dip (violet circles) appears. The increased dip separation and the development of a new dip at large incident angles signify the strong coupling of the two excitonic transitions with the SPP mode.

To understand the effects, we calculated the theoretical angle-dependent reflectance spectra using TMM presented in the 2D

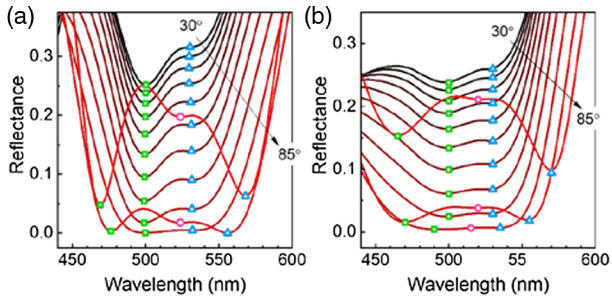

Fig. 2. (a) Theoretical and (b) experimental angle-dependent reflectance spectra for p-polarized light of the PMMA:R6G coated HMM structure. The incident angles range from 30° to 85° in 5° increments. The green squares, blue triangles, and violet circles denote the reflectance dips associated with the two R6G exciton modes and their interactions with the SPP modes at the large incident angles.

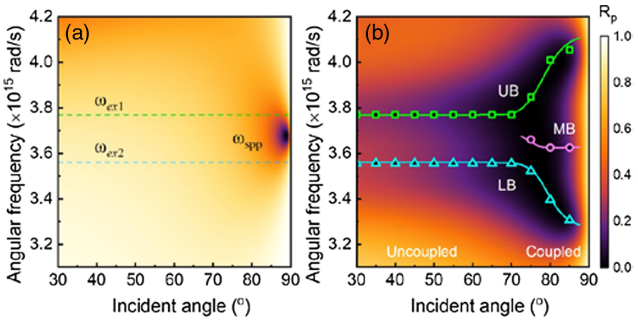

Fig. 3. Angle-dependent reflectance spectra for p-polarized light of the HMM sample coated with a 170 nm thick (a) undoped PMMA and (b) PMMA:R6G layer. The green and blue dashed lines overlaid in (a) indicate the angular frequencies of the two uncoupled exciton modes ω_{ex1} and ω_{ex2} positioned nearby the SPP mode ω_{spp}. The green, blue, and violet markers in (b) denote the experimental reflectance dips acquired from Fig. 2(b). The green, blue, and violet traces through them are the upper branch (UB), lower branch (LB), and middle branch (MB), respectively, obtained from the strong coupling fit based on the three eigenvalues of the Hamiltonian matrix in Eq. (3). Color code on the density plot represents the reflectance magnitude.

density plots in Fig. 3. Fig. 3(a) and Fig. S4(a) in Supplement 1 show that the HMM sample, coated with a 170 nm undoped PMMA film, exhibits a strong resonance dip occurring within an angular frequency ω_{spp} around 3.68×10^{15} rad/s or a wavelength at 512 nm. The resonance dip is not observable until the angle exceeds 75° and grows as the angle approaches 90°. The wavelength-selective SPP mode in this structure is the result of the indirect excitation of the SPP mode by a guided mode within the polymer film. The guided mode can only be excited at a large gliding incident angle without the help of prisms or grating structures, which explains the lack of angular dependence in ω_{spp} over a wide range of angles. This explanation is supported by the field distributions obtained from COMSOL simulations for an angle of incidence of 85° (Fig. S5 in Supplement 1). The electric field distribution shows that the propagating wave on the HMM surface is confined between the topmost unit cell of the HMM and the PMMA:R6G cladding layer.

The theoretical angle-dependent reflectance spectra in Fig. 3(b) show that the presence of R6G doping in the PMMA cladding creates two exciton branches at 3.56×10^{15} rad/s (530 nm) and 3.77×10^{15} rad/s (500 nm) associated with the vibronic transitions in R6G dye molecules [21]. The two branches start to separate farther apart when they overlap the guided SPP mode at the angles beyond 75°. As the angle approaches 90°, the surface plasmon resonance grows stronger [also shown in Fig. 3(a)], leading to intensified strong coupling. As a result, the energy difference between the two branches is maximized near 90°, and an additional middle branch appears. The presence of the three coupled states is the result of the interaction between the two exciton modes from R6G and a SPP mode from HMM. The measured angular reflectance minima acquired from Fig. 2(b) are presented with the theoretical results in Fig. 3(b) for comparison. The experimental data indicated by the green squares, blue triangles, and violet circles follow the low reflectance regions on the density plot and form the polaritonic branches of the coupled states. Figures S6(a) and S6(b) in Supplement 1 provide detailed experimental data with a smaller angular interval at large incident angles. Comparing the result with a reference sample with $\omega_{spp} = 3.25 \times 10^{15}$ rad/s far off the two exciton modes [Fig. S6(c) in Supplement 1] further confirms the presence of strong coupling. In this off-resonance mode, we clearly distinguish all three uncoupled oscillators.

The strong coupling process between the SPP mode on the HMM and the two molecular excitons from the $S_0 \rightarrow S_1$ vibronic transitions of the R6G absorption band can be described by using a quantum three-state model. The coupled states as functions of photon energy $E = \hbar\omega$ in the system are predicted by the eigenvalues of the Hamiltonian matrix,

$$\hat{H} = \begin{pmatrix} \bar{E}_{spp} & \Delta_1 & \Delta_2 \\ \Delta_1 & \bar{E}_{ex1} & 0 \\ \Delta_2 & 0 & \bar{E}_{ex2} \end{pmatrix}, \tag{3}$$

where $\bar{E}_{spp} = E_{spp} - i\Gamma_{spp}/2$ and $\bar{E}_{exj} = E_{exj} - i\Gamma_{exj}/2$ ($j = 1, 2$) denote the complex energies of the SPP and the two molecular excitons in R6G, respectively. The oscillator energies are centered at $E_{spp} = \hbar\omega_{spp}$ and $E_{exj} = \hbar\omega_{exj}$ with the linewidths of $\Gamma_{spp} = \hbar\gamma_{spp}$ and $\Gamma_{exj} = \hbar\gamma_{exj}$. The parameters $\Delta_j = \hbar\delta_j$ represent the two coupling energies between the SPP mode and the two excitonic modes. The eigenvalues of the Hamiltonian matrix give rise to three functions representing the upper, middle, and lower polaritonic branches of the coupled system.

To adequately express the SPP mode observed in Fig. 3(a) or Fig. S4(a) in Supplement 1 for the calculation of eigenvalues, we introduced a phenomenological function $p(\theta) = 1/\{1 + \exp[(\theta - \theta_0)/b]\}$ to illustrate its angle-dependent property. The emergence of the SPP mode with the resonance peak becoming sharper at large incident angles can be described by a fixed angular frequency around $\omega_{spp} = 3.68 \times 10^{15}$ rad/s with a damping frequency $\gamma_{spp}(\theta)$, which decreases as the light incident angle θ approaches 90°. Specifically, $\gamma_{spp}(\theta) = \gamma_{spp,90°}(1 + 3p(\theta))$. The parameters in $p(\theta)$, $\theta_0 = 77.5°$ and $b = 3$, were obtained by fitting experimental data. The parameter $\gamma_{spp}(\theta)$ is defined to remain large at small angles, decreases as θ increases beyond 75°, and reduces to a minimal damping frequency $\gamma_{spp,90°} = 2.82 \times 10^{14}$ rad/s measured at θ near 90°.

The same phenomenological function $p(\theta)$ is simultaneously applied to generate the angle-dependent coupling energies

$\hbar\delta_i(\theta)$. The treatment is based on the fact that the exciton–plasmon interaction only occurs when the SPP is available at the large incident angles. Therefore, the coupling energies scale with the strength of the surface plasmon resonance as the incident angle varies. Specifically, we define $\delta_j(\theta) = \delta_{j,\max}(1 - p(\theta))$ such that the coupling energy stays zero until the incident angle θ exceeds 75° and reaches a maximal value $\delta_{j,\max}$ as θ increases to 90°. From data fitting, we then extract $\delta_{1,\max}$ and $\delta_{2,\max}$ associated with the maximal interaction energies between the surface plasmon resonance and two exciton modes.

Using the measured angular frequencies and linewidths of the two exciton resonances ($\omega_{ex1} = 3.77 \times 10^{15}$ rad/s, $\gamma_{ex1} = 7.10 \times 10^{14}$ rad/s, $\omega_{ex2} = 3.56 \times 10^{15}$ rad/s, and $\gamma_{ex2} = 7.50 \times 10^{14}$ rad/s), and the known property of the SPP mode $\omega_{spp} = 3.68 \times 10^{15}$ rad/s and $\gamma_{spp,90°} = 2.82 \times 10^{14}$ rad/s near 90°, we extracted the coupling energies in the eigenvalues of the Hamiltonian matrix $\hat{H}$ to be $\delta_{1,\max} = 3.5 \times 10^{14}$ rad/s and $\delta_{2,\max} = 2.4 \times 10^{14}$ rad/s. The resulting eigenvalues forming the upper (UB), middle (MB), and lower (LB) branches are shown as the solid green, violet, and blue traces, respectively, closely matching the experimental data. The UB and LB evolve from the two original excitonic angular frequencies of the uncoupled excitons from R6G dye molecules at ω_{ex1} and ω_{ex2}. They deviate to result in an increased energy splitting with respect to MB at the large angles where they overlap with the SPP, indicating the presence of strong coupling. Figure S7 in Supplement 1 shows the simulation results obtained for the strong coupling of R6G to HMM with a different concentration of R6G in the PMMA matrix, which demonstrates that our phenomenological coupling model works for different resonance conditions.

The strong coupling condition in Eq. (4) allows us to examine the interactions of the SPP with the two exciton modes [7],

$$4\delta_{j,\max}^2 > \frac{\gamma_{exj}^2}{2} + \frac{\gamma_{spp,90°}^2}{2} \quad (j = 1, 2). \tag{4}$$

Although the condition is derived from a two-oscillator system, it verifies if the energy splitting between two coupled modes is perceptible compared to the average of their linewidths. See the derivation in Supplement 1 for more details. The extracted parameters suggest that the coupling energy between the SPP and exciton 1 agrees with the strong coupling condition. In contrast, the energy separation between the coupled SPP and exciton 2 is comparable to their individual linewidths. The results support the evidence of strong coupling and confirm the observable energy splitting between the three branches at large angles.

To conclude, we observed for the first time, to the best of our knowledge, the direct strong coupling between the dye molecules and the SPP on top of a planar HMM. The strong coupling was evidenced by the splitting of the resonance peaks observed upon the interaction between SPP and two exciton modes. The energy separations resulting from these two interactions were justified to be greater or comparable to the average linewidth of the SPP mode and each exciton mode. The study will open the route of developing novel planar photonic or electronic devices with improved performance, based on the light–matter interactions in the strong coupling regime.

Funding. National Science Foundation (DMR-1808258, ECCS-1542101, ECCS-1810067).

Acknowledgment. We thank Dr. Brady Gibbons for his assistance on the VASE ellipsometer and Rick Presley and Chris Tasker on the RF sputtering tool. Part of this research was conducted at the Northwest Nanotechnology Infrastructure, a National Nanotechnology Coordinated Infrastructure site at Oregon State University supported in part by the National Science Foundation (ECCS-1542101) and in part by Oregon State University.

Disclosures. The authors declare no conflicts of interest.

See Supplement 1 for supporting content.

REFERENCES

1. W. D. Newman, C. L. Cortes, and Z. Jacob, J. Opt. Soc. Am. B **30**, 766 (2013).
2. Z. Jacob, I. I. Smolyaninov, and E. E. Narimanov, Appl. Phys. Lett. **100**, 181105 (2012).
3. M. A. Noginov, H. Li, Y. A. Barnakov, D. Dryden, G. Nataraj, G. Zhu, C. E. Bonner, M. Mayy, Z. Jacob, and E. E. Narimanov, Opt. Lett. **35**, 1863 (2010).
4. Z. Jacob, J.-Y. Kim, G. V. Naik, A. Boltasseva, E. E. Narimanov, and V. M. Shalaev, Appl. Phys. B **100**, 215 (2010).
5. L. Novotny, Am. J. Phys. **78**, 1199 (2010).
6. J. A. Hutchison, T. Schwartz, C. Genet, E. Devaux, and T. W. Ebbesen, Angew. Chem. Int. Ed. **51**, 1592 (2012).
7. P. Törmä and W. L. Barnes, Rep. Prog. Phys. **78**, 013901 (2014).
8. M. Liscidini, D. Gerace, D. Sanvitto, and D. Bajoni, Appl. Phys. Lett. **98**, 121118 (2011).
9. S. Pirotta, M. Patrini, M. Liscidini, M. Galli, G. Dacarro, G. Canazza, G. Guizzetti, D. Comoretto, and D. Bajoni, Appl. Phys. Lett. **104**, 051111 (2014).
10. P. Shekhar and Z. Jacob, Phys. Rev. B **90**, 045313 (2014).
11. F. Vaianella, J. M. Hamm, O. Hess, and B. Maes, ACS Photon. **5**, 2486 (2018).
12. E. Orgiu, J. George, J. A. Hutchison, E. Devaux, J. F. Dayen, B. Doudin, F. Stellacci, C. Genet, J. Schachenmayer, C. Genes, G. Pupillo, P. Samorì, and T. W. Ebbesen, Nat. Mater. **14**, 1123 (2015).
13. A. Thomas, J. George, A. Shalabney, M. Dryzhakov, S. J. Varma, J. Moran, T. Chervy, X. Zhong, E. Devaux, C. Genet, J. A. Hutchison, and T. W. Ebbesen, Angew. Chem. Int. Ed. **128**, 11634 (2016).
14. K. H. Krishna, K. V. Sreekanth, and G. Strangi, J. Opt. Soc. Am. B **33**, 1038 (2016).
15. E. D. Palik, *Handbook of Optical Constants of Solids I, II, and III* (Academic, 1998).
16. S. C. Rashleigh, Opt. Quantum Electron. **8**, 49 (1976).
17. E. K. Tanyi, H. Thuman, N. Brown, S. Koutsares, V. A. Podolskiy, and M. A. Noginov, Adv. Opt. Mater. **5**, 1600941 (2017).
18. M. V. Klein and T. E. Furtak, *Optics*, 2nd ed. (Wiley, 1986), p. 116.
19. T. U. Tumkur, L. Gu, J. K. Kitur, E. E. Narimanov, and M. A. Noginov, Appl. Phys. Lett. **100**, 161103 (2012).
20. V. N. Peters, C. Yang, S. Prayakarao, and M. A. Noginov, J. Opt. Soc. Am. B **36**, E132 (2019).
21. P. Venkateswarlu, M. C. George, Y. V. Rao, H. Jagannath, G. Chakrapani, and A. Miahnahri, Pramana **28**, 59 (1987).